Dieni et al., J Nanomater Mol Nanotechnol 2013, 2:6
http://dx.doi.org/10.4172/2324-8777.1000124

Journal of Nanomaterials & Molecular Nanotechnology

Research Article

A SCITECHNOL JOURNAL

Spherical Gold Nanoparticles Impede the Function of Bovine Serum Albumin *In vitro*: A New Consideration for Studies in Nanotoxicology

Christopher Anthony Dieni[1]*, Christopher John Lewis Stone[1], Maxwell Luke Armstrong[1], Neal Ingraham Callaghan[1] and Tyson James MacCormack[1]

Abstract

Suspensions of bovine serum albumin (BSA) and spherical gold nanoparticles were analyzed to determine if gold nanoparticles (nAu) affect the ligand binding properties of BSA. A range of diameters ofnAu with a carboxylic acid capping agent (nAu-cap) were tested, along with nanoparticles conjugatedto amine (nAu-NH_3^+) and carboxyl (nAu-COO^-) functional groups via a covalent polymer bridge.All nAu tested were found to affect BSA conformation as determined by intrinsic tryptophan fluorescence. Smaller diameters ofnAu-cap (30-50 nm), along with nAu-$NH_3^+$and nAu-COO^-, impeded the binding of 8-anilino-1-napthalenesulfonic acid (ANS) to BSA. Similarly, smaller diameters of nAu-cap tended to impede oleic acid binding to BSA, with a linear negative correlation observed between nAu-cap diameter and the dissociation constant (K_D) of oleic acid over the range of 40-80 nm. 80 nm nAu-cap impeded butanoic acid binding, and necessitated a high-resolution fluorescence assay. As with oleic acid, smaller diameters of nAu-cap tended to impede ibuprofen binding, but no significance could be established. nAu-NH_3^+ and nAu-COO^- reduced the binding of thyroxine and bilirubin to BSA, with nAu-COO^-having a more pronounced effect in both cases. Visible-light spectral scans determined that interactions between BSA and different sizes of nAu did not change significantly over the course of 1 week, as established by relatively stable wavelengths of maximum absorbance. In order to isolate strongly-interacting BSA oligomers, irreversible BSA aggregates, or strong BSA-nAu complexes induced by recruitment of BSA into the protein corona, BSA-nAu-cap suspensions were subjected to centrifugal filtration and native-PAGE, however, this methodology failed to detect any altered distribution of higher-molecular weight species of BSA compared to control (free of nAu), suggesting that any protein-protein or protein-nAu interactions that contribute to these altered properties of BSA are not irreversible and do not withstand high g-forces and/or electrophoresis.

Keywords

Bovine serum albumin; Ligand binding; Protein corona; Spherical gold nanoparticles

***Corresponding author:** Dr. Christopher Anthony Dieni, Department of Chemistry and Biochemistry, Mount Allison University, Barclay Chemistry Building, 63C York Street, Sackville, New Brunswick, Canada, E4L 1G8, Tel: 506-364-2588; Fax: 506-364-2455; E-mail: cdieni@mta.ca

Received: August 02, 2013 **Accepted:** September 30, 2013 **Published:** October 10, 2013

Introduction

Over the past two decades, the appearance of engineered nanomaterials (ENMs) across multiple facets of science has surged at an ever-increasing rate [1,2]. Nanomaterials are now appearing as by-products of manufacturing processes [3], as biosensors and assay tools [4], as medical therapeutics [5], and in cosmetic products [6], among many otherapplications. Invariably, either through deliberate intent (e.g. the use of ENMs as therapeutics) or through incidental release and speciation in the environment, ENMs have found their way into a plethora of living organisms. Their potential detrimental effects have necessitated the rise of the field of nanotoxicology in order to study the mechanisms by which ENMs inflict damage, and ultimately, to establish proper regulations for their safe use and disposal [7].

ENMs have been found to exert their toxic effects in biological systems via two main mechanisms. One is the generation of reactive oxygen species and reactive nitrogen species [8-10]. These reactive species can then interact with numerous extracellular and intracellular components including metabolites, proteins, lipids, and DNA, damaging them and propagating reactive species even further. A second mechanism is through direct physical contact with biological molecules. In recent years it has become well-established that upon the introduction of ENMs into a biological fluid, a "protein corona" begins to form around them [11], comprised of the most prominent proteins within that fluid and/or the proteins which interact most favourably with the ENM. Proteins that form transient interactions with an ENM will initially form a "soft" and dynamic protein corona, ultimately yielding to a "hard" protein corona, composed of proteins with more stable and enduring interactions with ENMs [11,12]. These protein coronae effectively alter the surface properties of the ENMs, thereby influencing their overall disposition [11,13,14]; protein coronae can affect the distribution of ENMs between organ compartments and fluids, their uptake and ability to cross cell membranes, and their excretion.

While extensive research has been performed on the influence of protein coronae upon ENMs, the converse aspect- the effects on protein function following recruitment into coronae- are seldom examined. Our own previous work has demonstrated that the interaction of enzymes, with macromolecular structures (including ENMs) can significantly alter their regulation and function [15-17]. Several studies have investigated the conformational changes induced by recruitment of the most abundant plasma protein, serum albumin, into coronae, using either human serum albumin (HSA) or its homologues across the animal kingdom [14,18,19]. Conceivably, given that most known biomolecules (particularly proteins) exhibit stringent structure-function relationships, any conformational change of a protein induced by anENM will indeed have functional consequences. From a toxicity perspective, any localized perturbation of protein function could, in turn, have impacts on global physiology; Cedervall and colleagues demonstrated that polystyrene ENMs are transported up the food chain (from algae, to herbivores, and eventually to fish) and affect lipid metabolism in the top consumer, further specifying that the recruitment of apolipoprotein A1 into the corona disrupts the triglyceride: cholesterol ratio in fish [20].

In this report, we investigated the effects of spherical gold ENMs (nAu), on the ligand binding properties of bovine serum albumin (BSA). To assess the influence of ENM physicochemical properties on ligand binding, we tested nAu that varied in both diameter (nAu-cap, spanning 30-90 nm) and surface properties (nAu-$NH_3^+$and nAu-COO^-).

Materials and Methods

Nanoparticles and characterization

All gold ENMswere purchased from Nanopartz Inc. (Loveland, CO, USA). Three separate types of nAu were studied. To assess the influence of ENM size, we utilized nAu capped with a proprietary carboxylic acid(nAu-cap) of varying average diameters: 30 nm (specific sizes of lots used in this study, according to characterization information provided by the manufacturer: 31 and 33 nm), 40 nm (specific size: 42 nm), 50 nm (specific sizes: 51 and 52 nm), 60 nm (specific size: 58 nm), 70 nm (specific sizes: 69 and 70 nm), 80 nm (specific size:82 nm), and 90 nm (specific sizes: 87 and 90 nm).To assess the effects of nAu surface zeta potential (ζ potential) on BSA, we utilized 40 nm spherical nAu which were conjugated to either an amine polymer (positive ζ potential; nAu-NH_3^+) or a carboxyl polymer (negative ζ potential; nAu-COO^-).

Characterization information for each nAu formulation was provided by the manufacturer and included transmission electron microscopy images confirming nAu size and shape, dynamic light scattering measurements for hydrodynamic diameter, polydispersity, ζ potential, and absorbance spectra. Additional characterization was undertaken on 30, 50, 70, and 90 nm nAu-cap to support the data provided by the manufacturer(specific sizes of each nAu-cap lot used, according to characterization information reported by the manufacturer, were: 31, 51, 69 and 87 nm). Nanoparticle suspensions were diluted in 50 mM potassium phosphate buffer, pH 7.4, and absorbance spectra were collected using a NovaSpec Plus spectrophotometer (Biochrom Ltd., Cambridge, England). Hydrodynamic diameter was also measured in this subset of nAu formulationswith nanoparticle tracking analysis using a NanoSightLM10-HS (NanoSight Ltd. Amesbury, UK). Nanoparticles were suspended in 50 mM potassium phosphate buffer, pH 7.4, and diluted to between $1x10^8$-$8x10^8$ particles/mL prior to analysis. Size estimates are based on 255-7885 individual ENM tracks.

Reagents

All reagents were purchased from Sigma-Aldrich (St. Louis, MO, USA) unless otherwise specified.

Intrinsic tryptophan fluorescence of BSA

Alterations in BSA conformation were based on intrinsic fluorescence of tryptophan residues that change based on their local microenvironment (solvatochromic effect). Intrinsic tryptophan fluorescence was measured using an LS 50B fluorescence spectrometer (Perkin Elmer, Waltham, MA, USA) in single-cuvette format, with a 3 mL final volume. A 100 μM working solution of BSA was prepared in 50 mM sodium phosphate buffer, pH 7.4, and volumes of this working solution wereadded to cuvettes to ultimately yield a final concentration of 200 nM BSA. Control samples (in absence of nAu) were brought to a final volume of 3 mL with 50 mM sodium phosphate buffer, pH 7.4; alternatively, stock nAu-cap suspensions were added to cuvettes after BSA, in volumes that yielded a standard final concentration of 1 mg/L for each size of nAu-cap, followed by addition of phosphate buffer to a final sample volume of 3 mL. Cuvettes were mixed by inverting and fluorescence was measured at 280/350 nm (ex/em).

Intrinsic tryptophan fluorescence was also measured in the presence of nAu-NH_3^+or nAu-COO^-. Cuvette samples contained final concentrations of 2 μM BSA and 5 mg/L or 10 mg/L nAu-NH_3^+or nAu-COO^-, with final volumes equalized using 50 mM sodium phosphate buffer, pH 7.4. Cuvettes were mixed by inverting and fluorescence was measured at 280/350 nm (ex/em).

BSA ligand binding assays

Binding assays were conducted in microplate format using aSpectraMax M5 Multi-Mode microplate reader (Molecular Devices, Sunnyvale, CA, USA) and black opaque 96 well half area microplates (Greiner Bio-One, Monroe, NC, USA). These assays were based on the principle of an increase in fluorescence emission of a fluorescent probe, 8-anilino-1-napthalenesulfonic acid (ANS), upon entering a more hydrophobic environment (e.g. interacting with a BSA binding site). Optimal conditions for ANS saturation were first determined by varying ANS concentration over a range of 0-30 μM while holding BSA at a concentration of 540nM, using 50 mM sodium phosphate buffer, pH 7.4, to equalize final volumes. ANS fluorescence was measured at 372/475 nm (ex/em); saturating concentrations of ANS were determined from the fluorescence plateau of the binding curve.

Upon determining an appropriate saturating concentration of ANS (16 μM), experiments were carried out to determine whether nAu impeded binding of ANS to BSA at saturating ANS concentrations. Suspensions of 800nM BSA and 7.4 mg/L ofeach size of nAu-cap were prepared, and incubated for approximately 12 h at 4ºC; control suspensions were also prepared in absence of nAu. Following incubation, samples of eachsuspension were added to a 400 μM ANS working solution directly within black opaque microplates, and 50 mM sodium phosphate buffer, pH 7.4, was thenadded to bring each well to final volume. Final concentrations were: 540 nM BSA, 16 μM ANS, and 5 mg/L nAu (except for control assays, in which nAu was absent). Microplates were mixed in the SpectraMax M5 microplate reader, and fluorescence was measured at 372/475 nm (ex/em). In parallel, additional assays were prepared with 400 μM ANS, and the absence (control) or presence of 5 mg/L nAu-cap, but without BSA, using ethanol to bring each well to final volume rather than phosphate buffer; the hydrophobic character of ethanol in these assay wells induced ANS fluorescence, as would occur if ANS had been binding to BSA. However, with the omission of BSA, these additional assays served to determine any direct effect of nAu on ANS fluorescence, rather than a binding-dependent effect on ANS fluorescence mediated via BSA.

Binding of oleic acid (a high-affinity, long-chain fatty acid ligand) and butanoic acid (a low-affinity, short-chain fatty acid ligand) to BSA were assessed by utilizing ANS as a competitive fluorescent probe. Suspensions of BSA in absence or presence of nAu-cap were prepared as above, and incubated at 4ºC for 12 h. Samples of each suspension were then added to saturating concentrations of ANS (once again producing final concentrations of 540 nM BSA, 16 μM ANS, and 5 mg/L nAu-cap, except for control assays where nAu was absent). Prior to addition of phosphate buffer, however, a concentration range of either oleic acid (final concentrations of 0-16.5 μM from a 100 μM stock solution) or butanoic acid (final concentrations of

0-4 mM, from a 20 mM stock solution) was added to the BSA-nAu-ANS mixture, followed by equalizing volumes of phosphate buffer. Microplates were mixed in the SpectraMax M5 microplate reader, and fluorescence was measured at 372/475 nm (ex/em); changes in fluorescence caused by the displacementof ANS from binding sites on BSA were plotted against metabolite concentration (oleic or butanoic acid), and dissociation constants (K_D) were determined for each metabolite and for each nanoparticle-based condition (control, different nAu sizes).

Ibuprofen was used as a model pharmaceutical ligand of BSA. Binding of ibuprofen to BSA was assessed by utilizing the quenching of intrinsic tryptophan fluorescence upon ligand binding. Suspensions of BSA in absence or presence of nAu-cap were prepared as above, except that BSA concentration in these suspensions was increased to 50 μM, and incubated at 4ºC for 12 h. Samples of each suspension were then added to microplate wells for final concentrations of 10 μM BSA and 5 mg/L nAu-cap (except for control assays where nAu was absent). A concentration range of ibuprofen (final concentrations of 0-170 μM from a 500 μM stock solution) was added to each BSA-nAu suspension, followed by equalizing volumes of phosphate buffer. Microplates were mixed in the SpectraMax M5 microplate reader, and fluorescence was measured at 280/350 nm (ex/em); changes in intrinsic tryptophan fluorescence caused by ibuprofen binding were plotted against ibuprofen concentration, and K_D values were determined for each nanoparticle-based condition (control, different nAu-cap sizes).

Effect of nAu surface functionalization

Binding assays investigating the effects of nAu ζ potential were assessed using nAu-NH_3^+ and nAu-COO^-. Ligand binding assays were conducted using the LS 50B fluorescence spectrometer in single-cuvette format, with a 3 mL final volume. Optimal conditions for ANS saturation in this situation were first determined by varying ANS concentration over a range of 0-10 μM while holding BSA at a concentration of 500 nM, using 50 mM sodium phosphate buffer, pH 7.4, to equalize final volumes. ANS fluorescence was measured at 372/475 nm (ex/em).

Upon determining an appropriate saturating concentration of ANS (10μM), experiments were carried out to determine whether nAu impeded binding of ANS to BSA at saturating ANS concentrations. nAu-NH_3^+ or nAu-COO^- were directly added to cuvettes first, followed by ANS, BSA, and 50 mM sodium phosphate buffer, pH 7.4, to bring each cuvette sample to equal final volume. Final concentrations were: 500 nM BSA, 10 μM ANS, and 5 or 10 mg/L nAu (except for control assays, in which nAu was absent). Cuvettes were mixed by inverting, and fluorescence was measured at 372/475 nm (ex/em).

Binding of thyroxine (a model steroid hormone, which is a ligand of albumin) and bilirubin (a model toxic hydrophobic metabolite, which is also a ligand of BSA) to BSA were assessed by detecting the quenching of intrinsic tryptophan fluorescence upon ligand binding. nAu-NH_3^+ or nAu-COO^- were directly added to cuvettes first, followed by thyroxine or bilirubin, then BSA, and 50 mM sodium phosphate buffer, pH 7.4, to bring each cuvette sample to final volume. Final concentrations were: 2 μM BSA, 15 μM thyroxine or bilirubin, and 5 or 10 mg/L nAu (except for control assays, in which nAu was absent). Cuvettes were mixed by inverting and fluorescence was measured at 280/350 nm (ex/em). The decrease in intrinsic fluorescence or "quenching" induced by ligand (thyroxine or bilirubin) binding was determined in absence of nAu, and then contrasted with fluorescence quenching in the presence of 5 mg/L or 10 mg/L nAu-NH_3^+ or nAu-COO^-; computational corrections were made to take into account any intrinsic fluorescence quenching caused by nAu-NH_3^+ or nAu-COO^- alone (in absence of ligand binding).

High-resolution butanoic acid binding assay

The low affinity of BSA for butanoic acid and the reduced sensitivity of a microplate format for small fluorescence changes necessitated the use of an additional high-resolution assay for butanoic acid binding. The single-cuvetteLS 50B fluorescence spectrometer, with a longer path length, was used. Due to the low throughput nature of this assay, only 82 nm nAu-cap were investigated as they produced the most consistent changes in fluorescence in preliminary microplate-based assays. A 200 nM BSA solution was added to an 82 nm nAu-cap suspension directly within a cuvette; these were mixed by inversion and equilibrated at room temperature for 5 min. ANS was then added, followed by a concentration range of butanoic acid (0-575 μM from a 2 mM stock solution). 50 mM sodium phosphate buffer, pH 7.4, was used to equalize final volumes. Final concentrations were: 135 nM BSA, 6 μM ANS, and 1 mg/L nAu-cap (except for control assays, in which nAu was absent). Fluorescence was measured at 372/475 nm (ex/em); changes in fluorescence caused by the displacementof ANS from BSA were plotted against butanoic acid concentration, and K_D values were determined for control conditions versus presence of nAu-cap.

Visible-light spectral scans of BSA-nAu suspensions

BSA-nanoparticle suspensions were prepared containing 5 mg/mL BSA (from a 10 mg/mL stock) and 5 mg/LnAu-cap (specific sizes used were 31, 51, 69, and 87 nm, according to characterization information provided by manufacturer), and diluted to a final volume of 5 mL with 50 mM sodium phosphate buffer, pH 7.4; a control was prepared containing 5 mg/mL BSA in the absence of nAu. Immediately after preparation, 100 μLof each suspension was transferred to a clear polystyrene 96-well microplate (Greiner Bio-One, Monroe, NC, USA; Cat. No. 655101), and a visible-light (450-750 nm) absorbance spectrum scan was made using the Spectra Max M5microplate reader. Suspensions were incubated at 4ºC for 17 h and 186 h, at which point additional absorbance spectrum scans, were made.

Centrifugal filtration and electrophoresis of BSA-nAu suspensions

Centrifugal filtration and electrophoresis were utilized to investigate whether BSA-nAu-cap interactions were reversible, or if they resulted in irreversible protein-nAu-cap or protein-protein interactions, including protein aggregation. 500 μL of each suspension were applied to Amicon Ultra-0.5 mL 100K centrifugal filters (Millipore, Billerica, MA, USA) at each time point at which spectral scans were made (0 h, 17 h, 186 h). 100K-cutoff filters were chosen as this size would allow only monomeric BSA (~66.5 kDa) to pass through, but would trap any BSA species of higher molecular weight. Filter devices were centrifuged at 14,000 *x g* for 10 minutes, and retentate (the liquid which remained above the filter and did not pass through) was collected by centrifuging inverted filters at 1,000 *x g* for 2 minutes in a clean microfuge tube. Aliquots of filtrate and retentate were each mixed in a 1:1 ratio with 2x native-PAGE sample buffer (125 mM Tris, 20 % (v/v) glycerol, 0.1 % (w/v) bromophenol

blue). 40 µL of filtrate and 4 µL of retentate native-PAGE samples were loaded onto 7.5 % Mini-PROTEAN® TGX™ precast gels (Bio-Rad, Hercules, CA, USA) and gels were run in native-PAGE running buffer (25 mM Tris, 192 mM glycine), at a constant voltage of 160 V in a Mini-PROTEAN® Tetra Cell (Bio-Rad, Hercules, CA, USA), at -20ºC. Gels were stained using SimplyBlue™ Safestain (Life Technologies, Carlsbad, CA, USA; Cat. No. LC6060) according to the manufacturer's rapid staining protocol for minigels. Stained gels were imaged by white-light transillumination in a VersaDoc™ Imaging System (Bio-Rad, Hercules, CA, USA), and bands were quantified using the associated Quantity One® 1-D Analysis Software.

Results and Discussion

Nanoparticle characterization

The hydrodynamic diameters of a subset of nAu used in the study were determined using nanoparticle tracking analysis (Figure 1). 30, 50, 70, and 90 nm nAu-capwere examined in 50 mM potassium phosphate buffer (specific sizes of each nAu-cap lot that were used, according to characterization information provided by the manufacturer, were: 31, 51, 69 and 87 nm). Sufficient quantities of other nAu formulations used in the study were not available for analysis.All nAu-cap suspensions tested exhibited some polydispersity in buffer, as indicated by size distribution plots (Figure 1) and the variance associated with mean nAu-cap sizes (Table 1). As expected, the hydrodynamic diameters of 30, 50, and 70 nm nAu-capwere approximately 15-20 nm larger in buffer than in water, although the latter measurements (provided by the manufacturer) were taken using dynamic light scattering and hence may not be directly comparable. Hydrodynamic diameter is expected to increase with increasing ionic strength as the electrical double layer of the nAu particles is compressed and repulsive forces between individual particles decrease [21,22]. The minor increases that were observed in nAu-cap diameter in buffer vs. water suggest that aggregation was minimal. Our previous work has shown that even very polydisperse ENM suspensions with relatively large agglomerates (>300 nm) can affect protein structure and function [16]. The hydrodynamic diameter of 90 nm nAu-cap was consistent in buffer and water, making these nAu similar in mean size to the 70 nm nAu-capwhen suspended in buffer. It should also be noted that nanoparticle tracking analysis identified a population of smaller nAu-cap (c.a. 44 nm) in the90 nm nAu-cap suspension, but

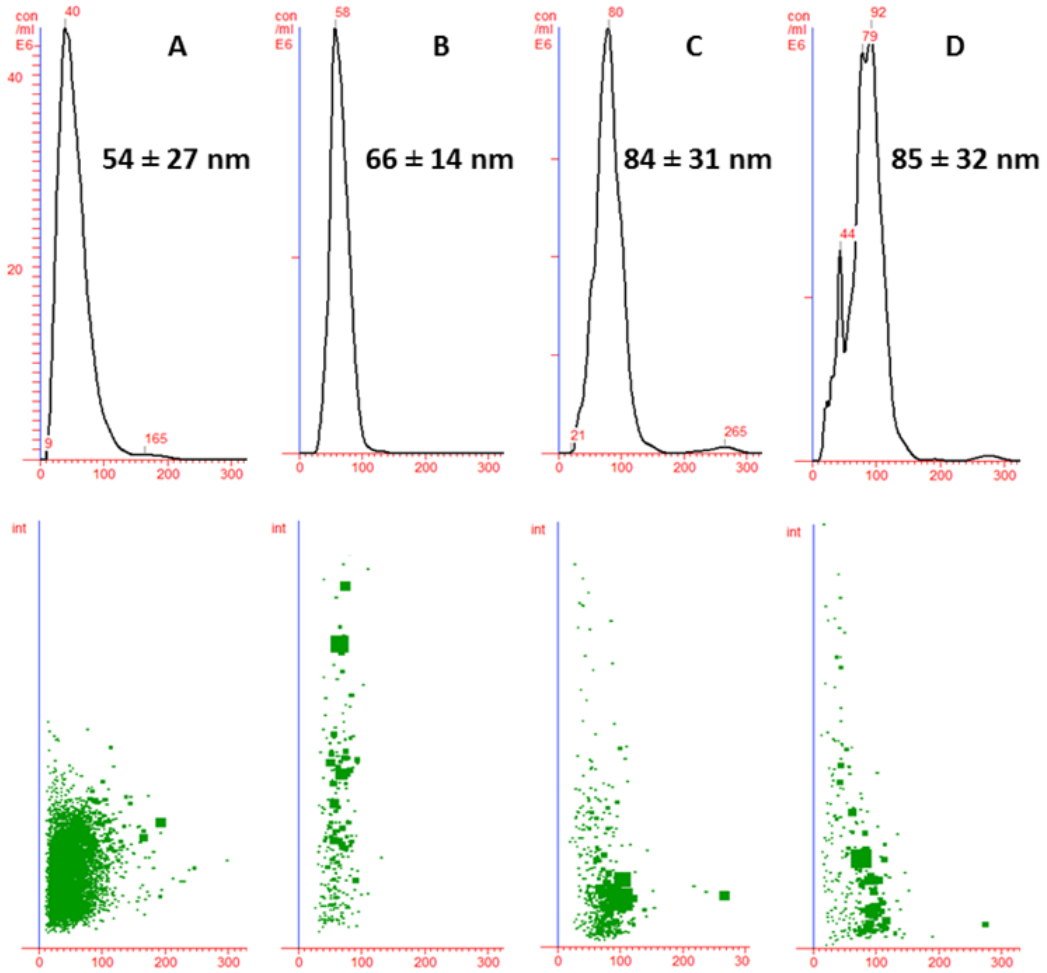

Figure 1: Hydrodynamic diameter (nm) of proprietary carboxylic acid-capped nAu (nAu-cap) in 50 mM potassium phosphate buffer (pH 7.4). Measurements were taken using NanoSight's Nanoparticle Tracking Analysis (NTA) software and are expressed as a function of concentration (top) and scattering intensity (bottom). Numerical values represent software-analyzed hydrodynamic diameter, means ± SD. Panels represent different sizes of nanoparticles: (A) 30 nm nAu-cap, (B) 50 nm nAu-cap, (C) 70 nm nAu-cap, and (D) 90 nm nAu-cap.

the significance of this finding is unclear in the context of effects on ligand binding. Absorbance spectra characteristics from 30, 50, 70, and 90 nm nAu-cap in buffer matched well with those provided by the manufacturer (data not shown), as did λ_{max} values (Table 1).

Effect of nAu-capsize on conformational and general binding properties of BSA

Several recent studies have shown that the properties of the protein corona- and the proteins comprising that corona- are influenced by ENMsize [11,13,18]. To determine the effects of various ENMsizes on the general conformational and binding properties of BSA, intrinsic tryptophan fluorescence and ANS fluorescence were both assayed in absence (control) and presence of each size of nAu-cap. The presence of nAu-capaffected intrinsic tryptophan fluorescence of BSA in a linear, size-dependent manner is shown in figure 2. Larger nAu tended to increase BSA fluorescence to a level higher than that observed in controls, whereas smaller nAuconversely tended to decrease fluorescence, in a linear fashionacross 30 to 90 nm nAu-cap (R^2=0.6843; slope significantly different from zero, p=0.022). It should be noted that these calculations, and all following linear regression analyses in this study, were made using the diameters of each nAu-cap within the manufacturer's characterization information (e.g. 33, 42, 52, 58, 70, 82, and 90 nm) as opposed to the typical average diameter of each nAu-cap formulation (e.g. 30, 40, 50, 60, 70, 80, and 90 nm). Certain nAu-cap formulationsalso affected the fluorescence resulting from interactions between BSA and saturating concentrations of ANS (Figure 3A). While larger-sized nAu-cap, from 60 to 90 nm, did not appear to reduce ANS fluorescence below the level observed in controls, 50, 40, and 30 nm nAu-cap causedsignificantdecreases (p<0.001 in each case).To determine whether fluorescence possibly decreased as a result of the nAu-cap directly quenching ANS itself [23], rather than via an effecton BSA and its binding of ANS, saturating concentrations of ANS were suspended in ethanol (free of BSA) and incubated with nAu-cap. Relative to control conditions, the presence of nAu-cap had no effect on ANS fluorescence in ethanol, regardless of nAu-cap size (Figure 3B). This indicates that nAu alters BSA conformation (including that of its binding sites), and the resulting decrease in fluorescence is a result of decreased ANS binding.

nAuformulation	ζ potential (mV)	Diameter in H_2O (nm)	Diameter in buffer (nm)	λ_{max} in H_2O (nm)	λ_{max} in buffer (nm)
30	-38 ± 3.4	31 ± 1.5	56 ± 27	523 ± 1.5	527.5
40	-44.0	42.0	*n/t*	528.0	*n/t*
50	-38.5 ± 6.4	51.5 ± 0.7	66 ± 14	533.5 ± 0.7	535.0
60	-45.3	58.0	*n/t*	537.0	*n/t*
70	-37.5 ± 3.5	69.5 ± 0.7	84 ± 31	541.5 ± 0.7	542.5
80	-43.1	82.0	*n/t*	567.0	*n/t*
90	-33.5 ± 7.8	88.5 ± 2.1	85 ± 32	575.5 ± 17.7	558.5
nAu-NH_3^+	+5.0	40.0	*n/t*	532.0	541.0
nAu-COO^-	-51.0	40.0	*n/t*	535.0	538.0

Table 1: Characterization information for gold nanoparticles (nAu) utilized in the study. Proprietary carboxylic acid-capped nAu (nAu-cap) of different diameters are represented by 30-90 and amine and carboxylic acid polymer conjugated nAu are denoted as nAu-NH_3^+ and nAu-COO^-, respectively.Data on zeta (ζ) potential, hydrodynamic diameter in H_2O, and absorbance maximum (λ_{max}) in H_2O were provided by the manufacturer. In cases where multiple lots of an individual formulation were studied, data is presented as a mean ± SD of information provided for each lot. *n/t*, not tested.

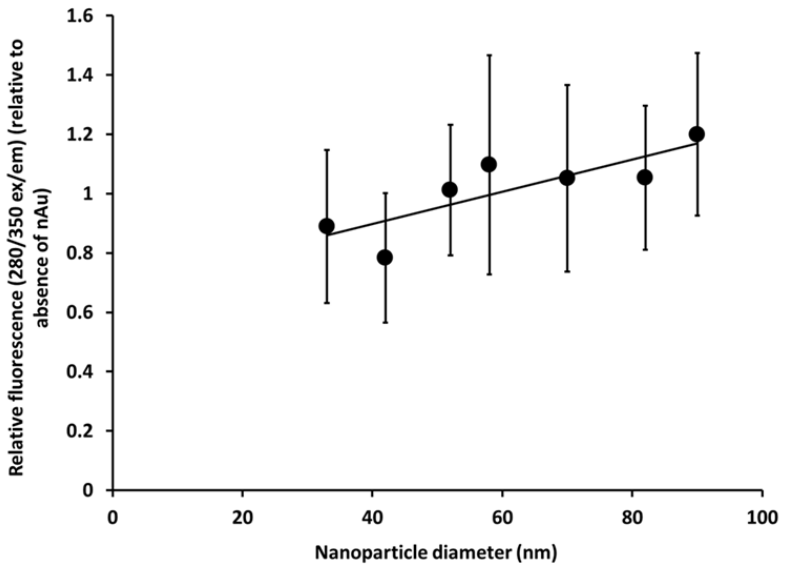

Figure 2: Effect of proprietary carboxylic acid-capped nAu (nAu-cap) on BSA conformation, as determined by intrinsic tryptophan fluorescence in presence of nanoparticles relative to fluorescence in absence of nanoparticles (control). Data points represent means ± SD, n=7 independent trials for each nanoparticle size. A linear relationship was observed between nanoparticle size and relative tryptophan fluorescence (R^2=0.6843; slope significantly different from zero, p=0.022).

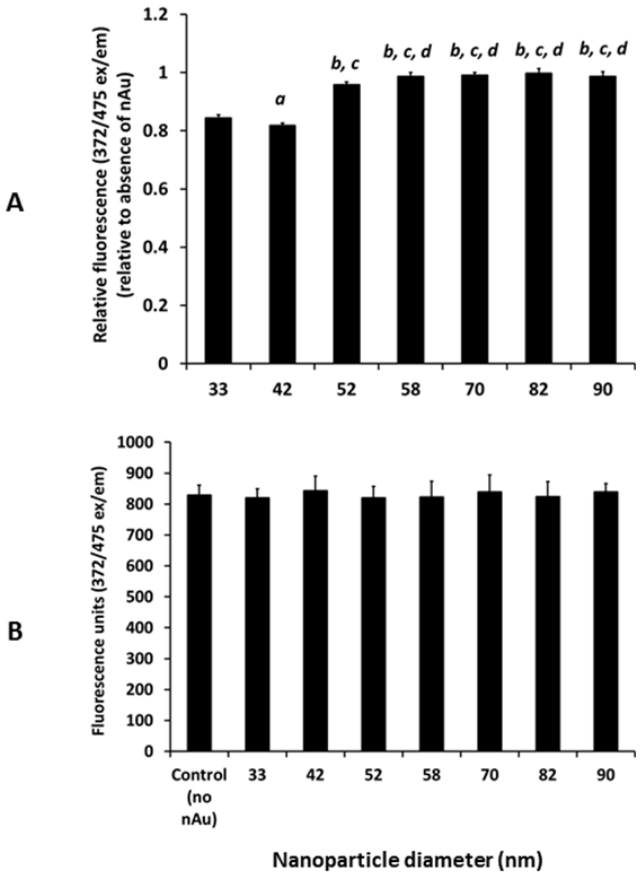

Figure 3: (A) Effect of proprietary carboxylic acid-capped nAu (nAu-cap) on maximal binding of ANS to BSA, as determined by maximum fluorescence of ANS in presence of nanoparticles relative to maximum fluorescence in absence of nanoparticles (control). Data points represent means ± SD, based on a minimum of 7 independent trials (n=7 for 33 nm nAu, and n=8 for all other sizes). Differences between groups were determined by one-way ANOVA followed by Tukey's multiple comparison test. Statistically significant differences between groups were as follows: different from presence of 33 nm nAu-cap, p<0.01 (*a*) or p<0.001 (*b*); (*c*) different from presence of 42 nm nAu-cap, p<0.001; (*d*) different from presence of 52 nm nAu-cap, p<0.001. (B) Effect of nAu-cap in ANS fluorescence in ethanol, n=3 independent trials for control and for each nanoparticle size.

Effect of nAu-capsize on binding of metabolites to BSA

The binding of three metabolites to BSA was tested in absence and presence of these various sizes of nAu-cap: oleic acid, butanoic acid, and ibuprofen. Fatty acids are known to have three primary and two secondary binding sites on BSA [24], whereas ibuprofen has at least one well-established binding site [25]. Of all sizes tested, only the 40 nm nAu-cap affected oleic acid binding to BSA such that a significantly higher (p<0.001) K_D was observed when compared to the control (Figure 4). Other differences were observedbetween individual nAu-cap formulations, but not between nAu-cap formulations and controls; while the K_D for oleic acid was not significantly altered by 30, 50, 60, 70, or 80 nm nAu-cap relative tocontrols, a distinct negative linear correlation was observed between K_D and nanoparticle size over the range of 40-80 nm nAu-cap (Figure 4 inset; R^2=0.8924, slope significantly different from zero, p=0.016).

A high-resolution assay was needed to detect the binding of butanoic acid to BSA, due to their weak interaction and the resultingsmall change in fluorescence caused by competition between butanoic acid and ANS. Standard microplate-scale assays that were used for other assessments above (including oleic acid binding) only allowed for moderately-reproducible measurements of a K_D butanoic acid, at best, and largely showed no clearly-defined relationship between butanoic acid concentration and fluorescence change. A possible effect on binding in the presence of 80 nm nAu-cap was observed (data not shown) so a modified, high-resolution ligand binding assay was performed. A cuvette-based assay was used in place of a microplate assay, allowing for a longer path length and greater sensitivity to better assess the effects of 80 nm nAu on butanoic acid binding. Using this assay, it was determined that the presence of 80 nm nAu significantly (p<0.001) increased the K_D of butanoic acid (Figure 5).

Finally, several sizes of nAu-captended to inhibit ibuprofen binding, as determined by changes in the K_D of ibuprofen are shown in figure 6. Most prominent were 40, 50, and 90 nm nAu-cap, which tended to increase K_D ibuprofen, and 80 nm nAu-cap, which tended to decrease K_D ibuprofen. However, the values obtained were quite variable, and no statistical significance was observed.

Effect of nAu surface functionalization on ligand binding properties of BSA

Protein coronae of ENMs can be influenced not only by ENM size, but by surface properties (e.g. ionic functionalizations) as well [12,19].To investigate the influence of ζ potential on the ligand binding properties of BSA, intrinsic tryptophan fluorescence and

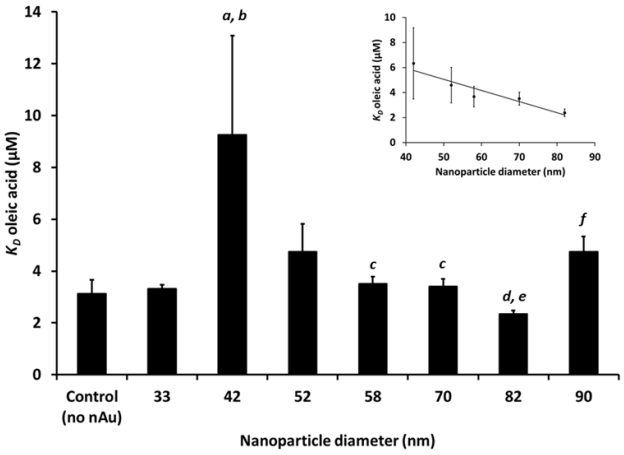

Figure 4: Effect of proprietary carboxylic acid-capped nAu (nAu-cap) on binding of oleic acid to BSA, as determined by dissociation constant (K_D). Data points represent means ± SEM, based on nonlinear fits of a minimum of 5 independently-prepared binding curves for each condition (n=5 independent trials for 42 nm nAu-cap, 7 independent trials for 52 nm and 90 nm nAu-cap, and 8 independent trials for control and all other sizes of nAu-cap). Differences between groups were determined by one-way ANOVA followed by Tukey's multiple comparison test. Statistically significant differences between groups were as follows: (*a*) different from controls (absence of nAu), p<0.001; (*b*) different from presence of 33 nm nAu-cap, p<0.001; different from presence of 42 nm nAu-cap, p<0.01 (*c*) or p<0.001 (*d*); (*e*) different from presence of 52 nm nAu-cap, p<0.01; (*f*) different from presence of 82 nm nAu-cap, p<0.05. Inset: plot showing a size-dependent linear trend of decreasing K_D over a range of 42-82 nm nAu-cap. R^2=0.8924, slope significantly different from zero (p=0.016).

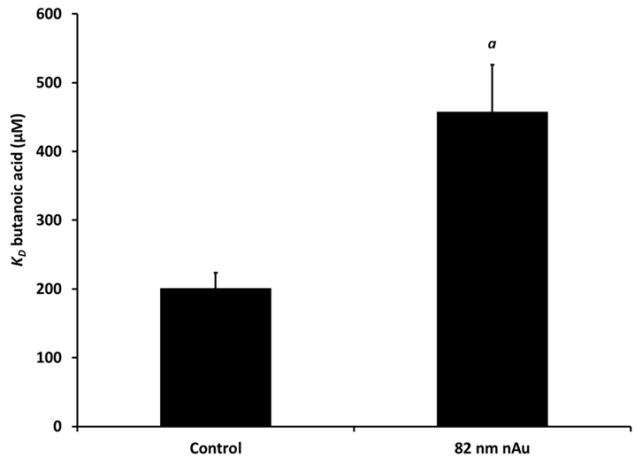

Figure 5: Effect of 82 nm nAu-cap on binding of butanoic acid to BSA, as determined by dissociation constant (K_D). Data points represent means ± SEM, based on nonlinear fits of a minimum of 5 independently-prepared binding curves for each condition (n=6 independent trials for control, 5 independent trials for 82 nm nAu-cap). Differences between groups were determined by one-way ANOVA followed by Tukey's multiple comparison test. Statistically significant differences between groups were as follows: (*a*) different from controls (absence of nAu), p<0.001.

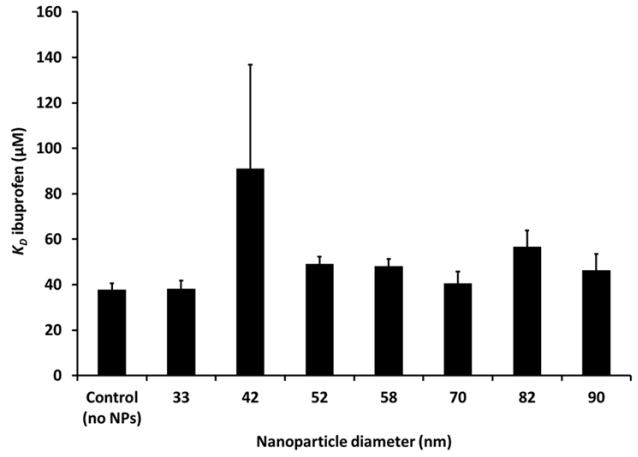

Figure 6: Effect of proprietary carboxylic acid-capped nAu (nAu-cap) on binding of ibuprofen to BSA, as determined by dissociation constant (K_D). Data points represent means ± SEM, based on nonlinear fits of a minimum of 5 independently-prepared binding curves for each condition (n=5 independent trials for 42 and 90 nm nAu-cap, 7 independent trials for 58, 70 and 82 nm nAu-cap, and 8 independent trials for control, 33 and 52 nm nAu-cap).

ANS fluorescence were assessed in the absence (control) or presence of nAu-NH_3^+ or nAu-COO^-.nAu-NH_3^+ had a ζ potential of +5.0 mV and nAu-COO^- had a ζ potential of -51.0 mV (Table 1). While nAu-NH_3^+did not significantly affect intrinsic tryptophan fluorescence of BSA, nAu-COO^- did affect fluorescence in a dose-dependent manner (Figure 7); 5 mg/L nAu-COO^- caused a tendency for intrinsic tryptophan fluorescence to decrease (but not significantly), whereas 10 mg/L caused a significant decrease (p<0.05).Despite BSA having a net negative surface potential at physiological pH, it has been previously indicated that BSA interacts with citrate caps on nAu via its lysine residues [26]. This suggests a possible mechanism by which anionic nAu influenced BSA conformation- and resulting intrinsic tryptophan fluorescence- to a greater extent than cationic nAu.Both nAu-NH_3^+ and nAu-COO^- also affected the fluorescence induced by the interactions between BSA and ANS (Figure 8), each in a dose-dependent manner.Decreases to ANS fluorescence caused by both nAu-NH_3^+ and nAu-COO^- were significant (p<0.05 or lower), with greater decreases once again caused by nAu-COO^- than by nAu-NH_3^+. When considering thatnAu-NH_3^+ did not affect tryptophan fluorescence, yet managed to affect ANS binding, it should be noted that ANS protein-binding is both a hydrophobic and electrostatic phenomenon, particularly due to ANS being an ionizable sulfonic acid [27]; thus, when dealing with ionic nanoparticle functionalizations, the binding of ANS and other ionizable ligands may be influenced by a combination of interactions between theENM and protein, as well as electrostatic interactions between the ENM and the ligand itself.

Effect of nAu surface functionalizations on binding of metabolites to BSA

The binding of two metabolites to BSA were tested in the absence and presence of nAu-NH_3^+ and nAu-COO^-: thyroxine and bilirubin. This assay was based on the quenching of intrinsic tryptophan fluorescence upon ligand binding. Therefore, when BSA is exposed to a ligand, a lower relative quenching may be indicative of decreased ligand binding, despite being at saturating concentrations.Once again, nAu-NH_3^+ and nAu-COO^- had differential effects on fluorescence quenching by thyroxine (Figure 9A).While nAu-NH_3^+ had no effect on fluorescence quenching at either concentration, 5 mg/L of nAu-COO^- significantly (p<0.001) reduced thyroxine's ability to quench intrinsic tryptophan fluorescence within BSA, suggesting impaired thyroxine binding. Curiously, however, when increased to 10 mg/L, a decrease

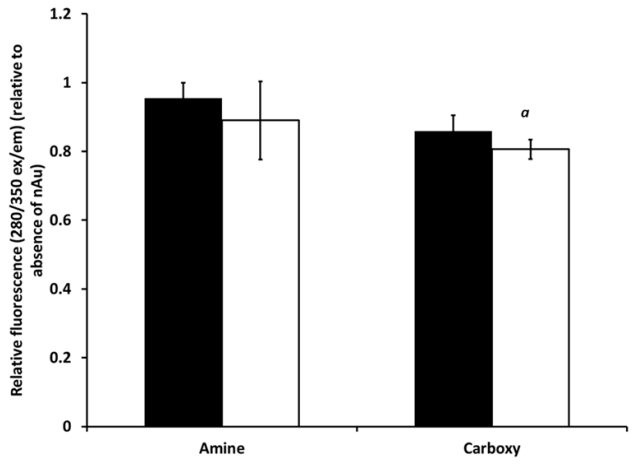

Figure 7: Effect of ionic nanoparticle functionalizations of amine (nAu-NH_3^+) and carboxylic acid (nAu-COO^-) polymer-conjugated nAu on BSA conformation, as determined by intrinsic tryptophan fluorescence in presence of nanoparticles relative to fluorescence in absence of nanoparticles (control). Data points represent means ± SD, n=3 independent trials for each nanoparticle functionalization and concentration; solid columns (■) represent 5 mg/L nAu, empty columns (□) represent 10 mg/L nAu. Differences between groups were determined by one-way ANOVA followed by Tukey's multiple comparison test.Statistically significant differences between groups were as follows: (*a*) different from controls (absence of nAu), p<0.05.

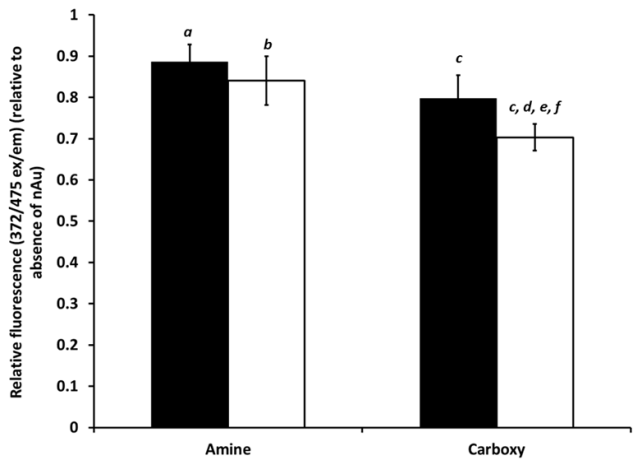

Figure 8: Effect of ionic nanoparticle functionalizations of amine (nAu-NH_3^+) and carboxylic acid (nAu-COO^-) polymer-conjugated nAuon maximal binding of ANS to BSA, as determined by maximum fluorescence of ANS in presence of nanoparticles relative to maximum fluorescence in absence of nanoparticles (control). Data points represent means ± SD, *n*=5 independent trials for each nanoparticle functionalization and concentration; solid columns (■) represent 5 mg/L nAu, open columns (□) represent 10 mg/L nAu. Differences between groups were determined by one-way ANOVA followed by Tukey's multiple comparison test. Statistically significant differences between groups were as follows: different from controls (absence of nAu), $p<0.05$ (*a*), $p<0.01$ (*b*), or $p<0.001$ (*c*); (*d*) different from presence of nAu-NH_3^+ at 5 mg/L, $p<0.001$; (*e*) different from presence of nAu-NH_3^+ at 10 mg/L, $p<0.01$; (*f*) different from presence of nAu-COO^- at 5 mg/L, $p<0.05$.

in fluorescence quenching was no longer detectable.The nAu-NH_3^+ and nAu-COO^- both significantly decreased fluorescence quenching by bilirubin ($p<0.01$; Figure 9B). While both functionalizations decreased fluorescence quenching, presumably by impeding bilirubin binding, nAu-COO^- had a significantly ($p<0.001$) greater effect than nAu-NH_3^+. No differences were observed between concentrations of 5 mg/L versus 10 mg/L for either of the given functionalizations.

Stability of the nAu-BSA interaction

Visible spectral scans of BSA-nAu-capsuspensions (30, 50, 70, and 90 nm nAu-cap) were taken immediately after preparation of the suspensions (0 h), after 17 h of incubation at 4ºC, and after over a week (186 h) at 4ºC (Figure 10). Any aggregation of nAu would have been spectrally-apparent by a red-shift in absorbance due to a change in surface plasmon resonance, resulting in an overall blue colour of the nanoparticles [28,29]. No significant differences were observed in the spectra for30, 50, 70, or 90 nm nAu-cap between any of the time points. While absolute absorbance values appeared to differ between time points in the typical spectra presented (most notably suspensions of BSA with 30 and 70 nm nAu-cap; Figure 10), after *n*=3 independent trials, no statistically significant differences could be identified.Wavelength of maximum absorption (λ_{max}) remained fairly constant over the entire period, and any given spectral scan detected neither any change greater than 7 nm in λ_{max} for any size nAu-cap at any time point, nor any reproducible pattern governing these changes (e.g. an either gradual decrease or increase in λ_{max} over time). Average λ_{max} over the 7-day period were determined to be 525 nm for 30 nm nAu-cap, 538 nm for 50 nm nAu-cap, 545 nm for 70 nm nAu-cap, and 557 nm for 90 nm nAu-cap. It should also be noted that the λ_{max} values for the 30, 50, and 70 nm nAu-cap in suspension with BSA were extremely similar the values observed for each respective nAu-cap size in H_2O or buffer (Table 1). We therefore surmise that over the 1-week period, protein coronae remained stable, based on the stability of nAu-cap.

In order to determine if "native" (and not only aggregative) interactions between proteins within a corona could be detected, samples from these incubations were then separated by centrifugal filtration in the hopes of isolating high-molecular weight species of BSA, indicative of protein-protein agglomeration induced by nanoparticles, and then electrophoresed by native-PAGE (Figure 11).Previous studies have employed methodology whereby ENMswere pelleted by centrifugation, washed extensively, and protein coronae were then analyzed via denaturing electrophoretic methods [12,13,19,26], though Cedervall and colleagues used size-exclusion chromatography in at least one instance because they found centrifugation-based methods too perturbing [18]; our intention in this studywas to capture any high-molecular weight species of BSA that may have formed as a result of strong intra- or inter- coronae protein-nAu or protein-protein interactions, including aggregations. For control conditions (absence of nAu), some fraction of the BSA monomeric species passed though the 100K-cutoff centrifugal filter (filtrate), while the retentate visibly consisted of the remaining fraction of BSA monomers (that had been concentrated and were

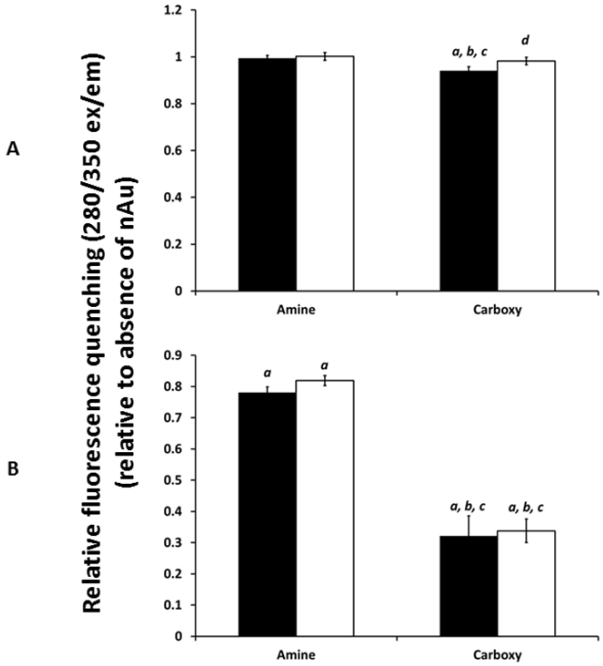

Figure 9: Effect of ionic nanoparticle functionalizations of amine (nAu-NH_3^+) and carboxylic acid (nAu-COO^-) polymer-conjugated nAu on binding of metabolites to BSA, as determined by quenching of intrinsic tryptophan fluorescence in presence of nanoparticles relative to quenching in absence of nanoparticles (control). Data points represent means ± SD, *n*=5 independent trials for each nanoparticle functionalization and concentration; solid columns (■) represent 5 mg/L nAu, open columns (□) represent 10 mg/L nAu. Panels represent (A) differences in thyroxine binding and (B) differences in bilirubin binding.Statistically significant differences between groups were determined by one-way ANOVA followed by Tukey's multiple comparison test, and were as follows: (*a*) different from controls (absence of nAu), $p<0.001$; (*b*) different from presence of nAu-NH_3^+ at 5 mg/L, $p<0.001$; (*c*) different from presence of nAu-NH_3^+ at 10 mg/L, $p<0.001$; (*d*) different from presence of nAu-COO^- at 5 mg/L, $p<0.01$.

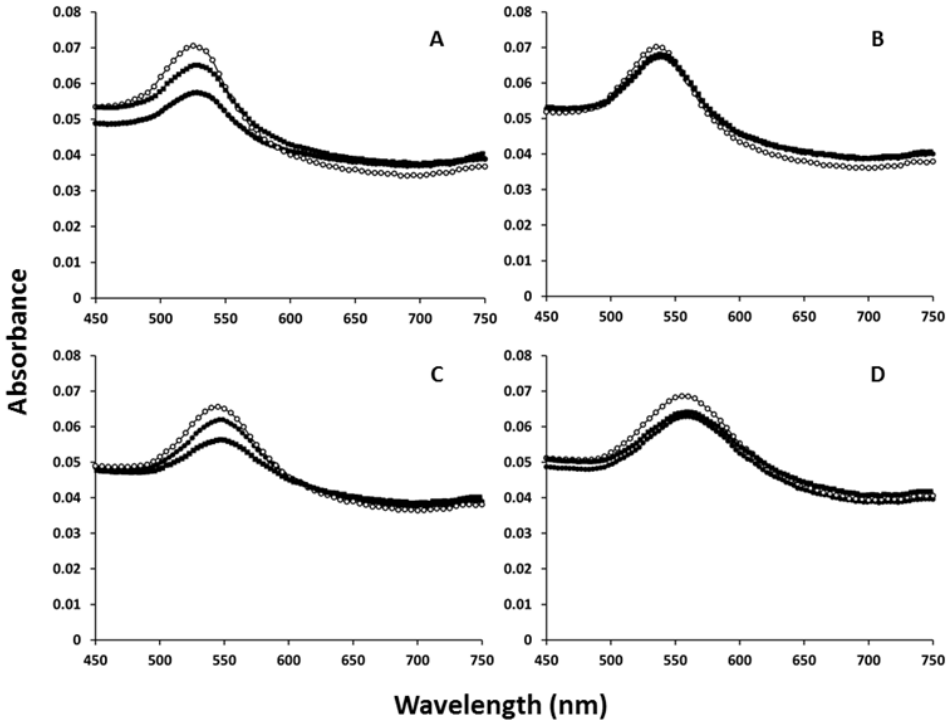

Figure 10: Typical absorbance spectral scans of BSA and proprietary carboxylic acid-capped nAu (nAu-cap) suspensions. Data points represent a single trial, however, *n*=3 independent trials for each nAu-capsize were carried out; solid circles (●) represent spectral scans immediately after preparing the suspension (0 h), open circles (○) represent spectral scans of the suspension after 17 h, and solid squares (■) represent spectral scans of the suspension after 186 h (over 1 week). While certain sizes of nAu-cap may appear to show changes in the absolute absorbance levels at different time points, any differences after *n*=3 trials were determined to be statistically insignificant. Panels represent suspensions of BSA and (A) 31 nm nAu, (B) 51 nm nAu, (C) 69 nm nAu, and (D) 87 nm nAu.

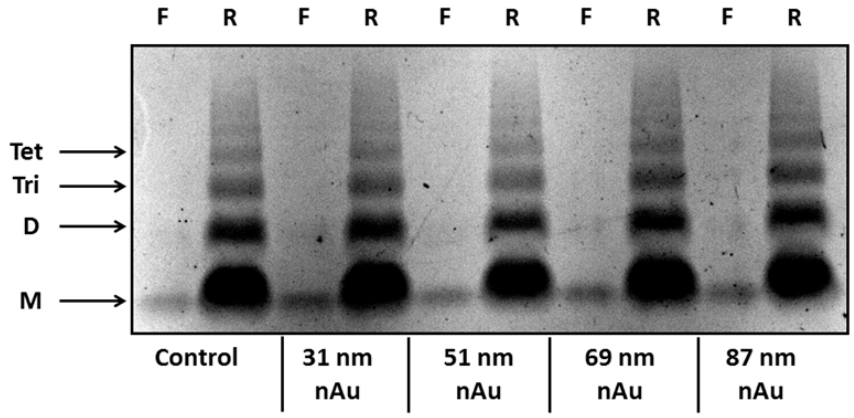

Figure 11: Typical image for a Simply Blue-stained native-PAGE of suspensions of BSA in absence of nAu (control) or in the presence of 31, 51, 69, or 87 nm proprietary carboxylic acid-capped nAu (nAu-cap), following centrifugal filtration. This image represents a single trial, however, *n*=3 independent trials for each nanoparticle size were carried out, and were filtered and electrophoresed at 0 h, 17 h, and 186 h. Symbols or abbreviations represent the following: (M) monomeric species of BSA; (D) dimeric species of BSA; (Tri) trimeric species of BSA; (Tet) tetrameric species of BSA; (F) filtrate which passed through the 100K-cutoff centrifugal filter; (R) retentate which was retained by the 100K-cutoff centrifugal filter.

thus much darker in intensity), as well bands corresponding in molecular weight to dimers, trimers, tetramers, and possibly other higher molecular weight species that were too faint to distinctly identify by this methodology. For samples containing 30, 50, 70, or 90 nm nAu-cap, these ENMs were present and concentrated in the retentate as observed byan intensified red colour, and a red band in gel lanes where nAu-containing retentate was loaded, which did not remain visible after gel staining.However, the electrophoretic pattern observed showed no differences between controls versus presence of any size of nAu-cap; no significant changes were observed in terms of i) the distribution of monomers between filtrate and retentate, ii) the preferential distribution of multimeric species, or iii) any appearance

of distinct or well-defined higher molecular weight species. This remained constant over *n*=3 independent preparations, regardless of the length of incubation (0 h, 17 h, 186 h).This would indicate that any protein-nAu or protein-protein interactions induced by nAu-capare either reversible or they were simply not detectable by our methodology.It is possible that the g-forces of the centrifugal filtration (10,000 x *g*) and/or the electrophoretic forces of non-denaturing-PAGEwere sufficient to reverse any protein-nAu or protein-protein interactions induced by these nAu-cap formulations.

Conclusions

In this study, we have attempted to lay the groundwork for what we feel is an important and, to-date, overlooked aspect of the nanoparticle protein corona: the recruitment of proteins into coronae and the resulting effects on protein function. We have shown that nAu alterthe conformation of BSA differently depending on their size, surface properties, and concentration; as a possible direct effect of this conformational change, the binding of fatty acids (oleic and butanoic acid), drugs (ibuprofen), hormones (thyroxine), and toxic metabolic breakdown products (bilirubin) may be significantly impaired. Future studies will focus on why the binding of some ligands was affected whereas those of other ligands were not, and why some ligand-binding exhibits clear relationships with certain nAu characteristics (e.g. linear relationship with size, concentration; preferential effect with anions versus cations) whereas others do not. One very recent study [14] has determined that HSA (the human homologue to BSA) has a geometry equivalent to that of an equilateral triangular prism, and that HSA preferentially binds to FePt nanoparticles via its triangular "face" rather than its "sides"; if this finding translates to the albumin of other species (such as BSA) and their interaction with other ENMs, it could explain why the binding properties of certain ligands are particularly affected by specific nAu formulations but not others.We also determined over the course of this study that the order which nAu, BSA, and ligand are added to one another, and the length of incubation prior to assay, can have a significant effect on the results; we did not emphasize these findings in our current report, but state this here as a cautionary that the mechanism of protein corona formation, and how those proteins may subsequently interact with their ligands, is likely even more complex than we currently suspect].

Acknowledgements

We would like to thank Dr. Suzanne Curriefor providingaccess to equipment used in the study. We would also like to thank Mr. Ian Chute and the Atlantic Cancer Research Institute forassistance with thenanoparticle tracking analysis. This research was funded by a Margaret and Wallace McCain Postdoctoral Fellowship to CAD, a Marjorie Young Bell Foundation fellowship to CJLS, a Cuthbertson fellowship to MLA, a Carnegie scholarship to NIC, and a Natural Sciences and Engineering Research Council of Canada Discovery Grant to TJM. The authors declare no conflict of interest in the work presented here.

References

1. Aitken RJ, Chaudhry MQ, Boxall AB, Hull M (2006) Manufacture and use of nanomaterials: current status in the UK and global trends. Occup Med (Lond) 56: 300-306.
2. Westerhoff P, Nowack B (2013) Searching for global descriptors of engineered nanomaterial fate and transport in the environment. Acc Chem Res 46: 844-853.
3. Park JY, Ramachandran G, Raynor PC, Kim SW (2011) Estimation of surface area concentration of workplace incidental nanoparticles based on number and mass concentrations. J Nanopart Res 13: 4897-4911.
4. Wang J (2005) Carbon-nanotube based electrochemical sensors: a review. Electroanal 17: 7-14.
5. Nie S (2010) Understanding and overcoming major barriers in cancer nanomedicine. Nanomedicine (Lond) 5: 523-528.
6. Mu L, Sprando RL (2010) Application of nanotechnology in cosmetics. Pharm Res 27: 1746-1749.
7. Jennifer M, Maciej W (2013) Nanoparticle technology as a double-edged sword: cytotoxic, genotoxic, and epigenetic effects on living cells. J Biomater Nanobiotechnol 4: 53-63.
8. Nel A, Xia T, Mädler L, Li N (2006) Toxic potential of materials at the nanolevel. Science 311: 622-627.
9. Xia T, Kovochich M, Liong M, Mädler L, Gilbert B, et al. (2008) Comparison of the mechanism of toxicity of zinc oxide and cerium oxide nanoparticles based on dissolution and oxidative stress properties. ACS Nano 2: 2121-2134.
10. Rasmussen JW, Martinez E, Louka P, Wingett DG (2010) Zinc oxide nanoparticles for selective destruction of tumor cells and potential for drug delivery applications. Expert Opin Drug Deliv 7: 1063-1077.
11. Rahman M, Laurent S, Tawil N, L'Hocine Y, Mahmoudi M (2013) Nanoparticle and protein corona. In: Protein-nanoparticle interactions: The bio-nano interface. Springer-Verlag Heidelberg, 21-44.
12. Lundqvist M, Stigler J, Elia G, Lynch I, Cedervall T, et al. (2008) Nanoparticle size and surface properties determine the protein corona with possible implications for biological impacts. Proc Natl Acad Sci U S A 105: 14265-14270.
13. Tenzer S, Docter D, Rosfa S, Wlodarski A, Kuharev J, et al. (2011) Nanoparticle size is a critical physicochemical determinant of the human blood plasma corona: a comprehensive quantitative proteomic analysis. ACS Nano 5: 7155-7167.
14. Nienhaus GU, Maffre P, Nienhaus K (2013) Studying the protein corona on nanoparticles by FCS. Methods Enzymol 519: 115-137.
15. Dieni CA, Storey KB (2008) Regulation of 5'-adenosine monophosphate deaminase in the freeze tolerant wood frog, Rana sylvatica. BMC Biochem 9: 12.
16. Maccormack TJ, Clark RJ, Dang MK, Ma G, Kelly JA, et al. (2012) Inhibition of enzyme activity by nanomaterials: potential mechanisms and implications for nanotoxicity testing. Nanotoxicology 6: 514-525.
17. Schultz AG, Ong KJ, MacCormack T, Ma G, Veinot JG, et al. (2012) Silver nanoparticles inhibit sodium uptake in juvenile rainbow trout (Oncorhynchus mykiss). Environ Sci Technol 46: 10295-10301.
18. Cedervall T, Lynch I, Lindman S, Berggård T, Thulin E, et al. (2007) Understanding the nanoparticle-protein corona using methods to quantify exchange rates and affinities of proteins for nanoparticles. Proc Natl Acad Sci U S A 104: 2050-2055.
19. Podila R, Chen R, Ke PC, Brown JM, Rao AM (2012) Effects of surface functional groups on the formation of nanoparticle-protein corona. Appl Phys Lett 101: 263701.
20. Cedervall T, Hansson LA, Lard M, Frohm B, Linse S (2012) Food chain transport of nanoparticles affects behaviour and fat metabolism in fish. PLoS One 7: e32254.
21. Derjaguin BV, Landau LD (1941) Theory of the stability of strongly charged lyophobic sols and of the adhesion of strongly charged particles in solutions of electrolytes. Acta Physicochim 14: 733-762.
22. Verwey EJW, Overbeek JTHG, van Nes K (1948) Theory of the stability of lyophobic colloids: the interaction of sol particles having an electric double layer. Elsevier Publishing.
23. Acuna GP, Bucher M, Stein IH, Steinhauer C, Kuzyk A, et al. (2012) Distance dependence of single-fluorophore quenching by gold nanoparticles studied on DNA origami. ACS Nano 6: 3189-3195.
24. Hamilton JA, Era S, Bhamidipati SP, Reed RG (1991) Locations of the three primary binding sites for long-chain fatty acids on bovine serum albumin. Proc Natl Acad Sci U S A 88: 2051-2054.
25. Ni Y, Su S, Kokot S (2006) Spectrofluorimetric studies on the binding of salicylic acid to bovine serum albumin using warfarin and ibuprofen as site markers with the aid of parallel factor analysis. Anal Chim Acta 580: 206-215.
26. Dominguez-Medina S, McDonough S, Swanglap P, Landes CF, Link S (2012) In situ measurement of bovine serum albumin interaction with gold nanospheres. Langmuir 28: 9131-9139.

27. Latypov RF, Liu D, Gunasekaran K, Harvey TS, Razinkov VI, et al. (2008) Structural and thermodynamic effects of ANS binding to human interleukin-1 receptor antagonist. Protein Sci 17: 652-663.

28. Elghanian R, Storhoff JJ, Mucic RC, Letsinger RL, Mirkin CA (1997) Selective colorimetric detection of polynucleotides based on the distance-dependent optical properties of gold nanoparticles. Science 277: 1078-1081.

29. Zhang S, Wang J, Han L, Li C, Wang W, et al. (2010) Colorimetric detection of bis-phosphorylated peptides using zinc(ii) dipicolylamine-appended gold nanoparticles. Sensor Actuat B-Chem 147: 687-690.

Author Affiliation

Top

[1]Department of Chemistry and Biochemistry, Mount Allison University, Canada